SINTEF
PROCEEDINGS
2

Proceedings of the 12th International Conference on Computational Fluid Dynamics in the Oil & Gas, Metallurgical and Process Industries

Progress in Applied CFD – CFD2017

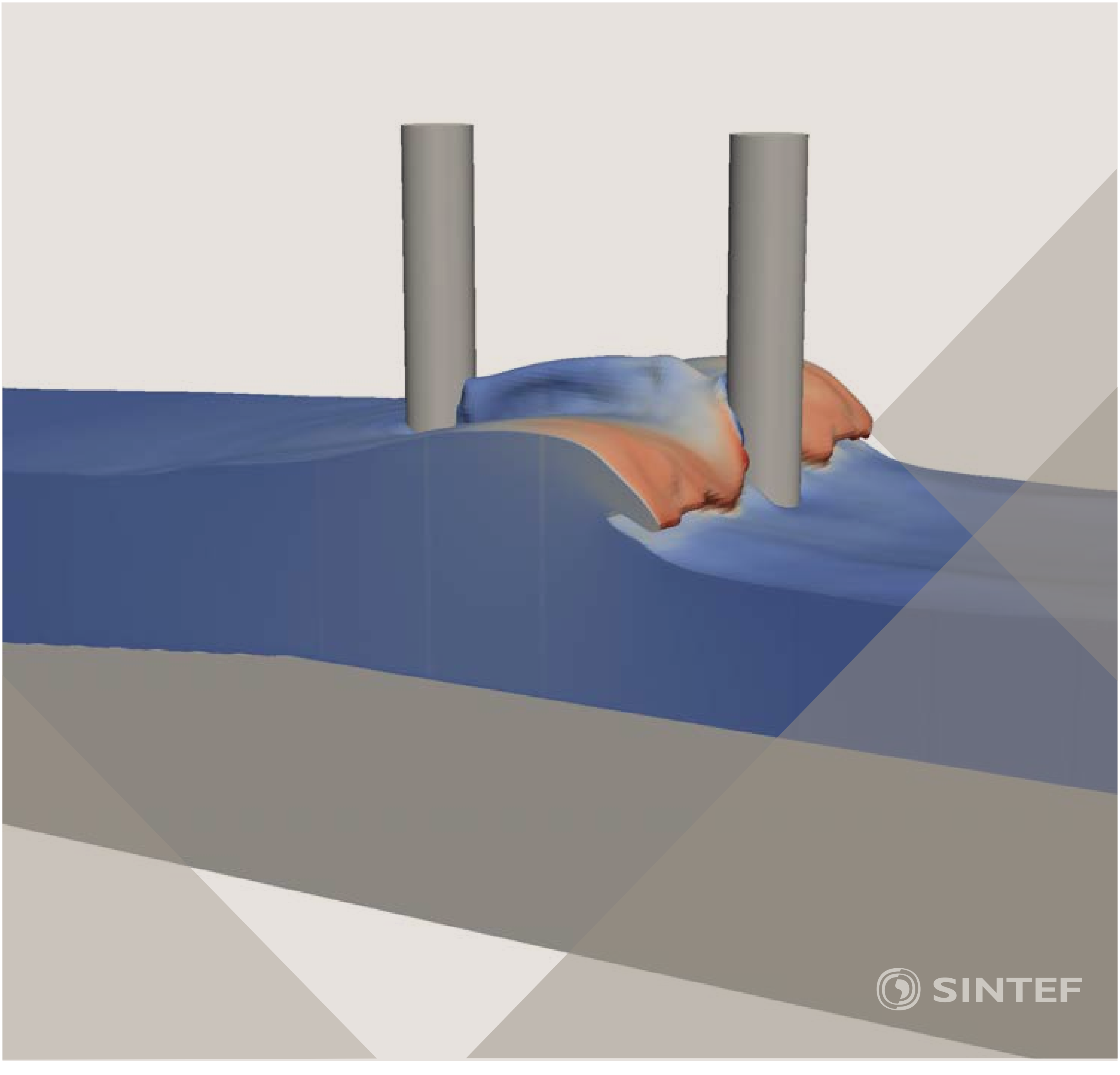

SINTEF

SINTEF Proceedings

Editors:
Jan Erik Olsen and Stein Tore Johansen

Progress in Applied CFD – CFD2017

Proceedings of the 12th International Conference on Computational Fluid Dynamics in the Oil & Gas, Metallurgical and Process Industries

SINTEF Academic Press

SINTEF Proceedings no 2
Editors: Jan Erik Olsen and Stein Tore Johansen

Progress in Applied CFD – CFD2017

Selected papers from 10th International Conference on Computational Fluid Dynamics in the Oil & Gas, Metallurgical and Process Industries

Key words:
CFD, Flow, Modelling

Cover, illustration: Arun Kamath

ISSN 2387-4295 (online)
ISBN 978-82-536-1544-8 (pdf)

SINTEF Academic Press

Address:	Forskningsveien 3 B
	PO Box 124 Blindern
	N-0314 OSLO
Tel:	+47 73 59 30 00
Fax:	+47 22 96 55 08

www.sintef.no/byggforsk
www.sintefbok.no

SINTEF Proceedings

SINTEF Proceedings is a serial publication for peer-reviewed conference proceedings on a variety of scientific topics.

The processes of peer-reviewing of papers published in SINTEF Proceedings are administered by the conference organizers and proceedings editors. Detailed procedures will vary according to custom and practice in each scientific community.

PREFACE

This book contains all manuscripts approved by the reviewers and the organizing committee of the 12th International Conference on Computational Fluid Dynamics in the Oil & Gas, Metallurgical and Process Industries. The conference was hosted by SINTEF in Trondheim in May/June 2017 and is also known as CFD2017 for short. The conference series was initiated by CSIRO and Phil Schwarz in 1997. So far the conference has been alternating between CSIRO in Melbourne and SINTEF in Trondheim. The conferences focuses on the application of CFD in the oil and gas industries, metal production, mineral processing, power generation, chemicals and other process industries. In addition pragmatic modelling concepts and bio-mechanical applications have become an important part of the conference. The papers in this book demonstrate the current progress in applied CFD.

The conference papers undergo a review process involving two experts. Only papers accepted by the reviewers are included in the proceedings. 108 contributions were presented at the conference together with six keynote presentations. A majority of these contributions are presented by their manuscript in this collection (a few were granted to present without an accompanying manuscript).

The organizing committee would like to thank everyone who has helped with review of manuscripts, all those who helped to promote the conference and all authors who have submitted scientific contributions. We are also grateful for the support from the conference sponsors: ANSYS, SFI Metal Production and NanoSim.

Stein Tore Johansen & Jan Erik Olsen

ANSYS®

metal production

NanoSim

Organizing committee:

Conference chairman: Prof. Stein Tore Johansen
Conference coordinator: Dr. Jan Erik Olsen
Dr. Bernhard Müller
Dr.Sigrid Karstad Dahl
Dr.Shahriar Amini
Dr.Ernst Meese
Dr.Josip Zoric
Dr.Jannike Solsvik
Dr.Peter Witt

Scientific committee:

Stein Tore Johansen, SINTEF/NTNU
Bernhard Müller, NTNU
Phil Schwarz, CSIRO
Akio Tomiyama, Kobe University
Hans Kuipers, Eindhoven University of Technology
Jinghai Li, Chinese Academy of Science
Markus Braun, Ansys
Simon Lo, CD-adapco
Patrick Segers, Universiteit Gent
Jiyuan Tu, RMIT
Jos Derksen, University of Aberdeen
Dmitry Eskin, Schlumberger-Doll Research
Pär Jönsson, KTH
Stefan Pirker, Johannes Kepler University
Josip Zoric, SINTEF

CONTENTS

MODELING OF FLUID DYNAMICS, MASS TRANSFER, AND CHEMICAL REACTION IN BUBBLY FLOWS

Roland Rzehak* **and Manuel Krauß**

Helmholtz-Zentrum Dresden - Rossendorf, Bautzner Landstrasse 400, 01328 Dresden, Germany

* E-mail: r.rzehak@hzdr.de

ABSTRACT

Mass transfer from gas bubbles to the surrounding liquid or vice versa is an important consideration in chemical engineering. Frequently such absorption or desorption processes are accompanied by a chemical reaction in the liquid phase. Compared with the fluid dynamics of bubbly flows, modeling and simulation of these processes is much less developed. The present work shows some recent advances made in validating closures for the Eulerian two-fluid framework of interpenetrating continua.

Keywords: dispersed gas liquid multiphase flow, Euler-Euler two-fluid model, CFD simulation, fluid dynamics, mass transfer, chemical reaction, absorption.

NOMENCLATURE

Greek Symbols

α	volume fraction [-]
μ	viscosity [Pa s]
ρ	density [kg m^{-3}]
σ	surface tension [N m^{-1}]

Latin Symbols

C^X	Molar concentration of species X [kmol m^{-3}]
d	bubble diameter [m]
D	column diameter [m]
D^X	diffusion coefficient of species X [m^2 s^{-1}]
E	enhancement factor [-]
Ha	Hatta number [-]
k	specific turbulent kinetic energy [m^2 s^{-2}]
k	mass transfer coefficient [m s^{-1}]
$k^{\Xi\pm}$	for- (+) and backward (-) rate constant of reaction Ξ with total reaction order ξ [(m^3 kmol^{-1})$^{\xi-1}$ s^{-1}]
H	column height [m]
R	pipe / column radius or halfwidth [m]
Re	Reynolds number [-]
Sc	Schmidt number [-]
$\mathbf{x}$	position [m]
$\mathbf{u}$	mean velocity [m s^{-1}]
$\mathbf{u'}$	fluctuating velocity [m s^{-1}]

Sub/superscripts

a	asymptotic limit of an instantaneous reaction
B	bubble
eff	effective
G	gas
L	liquid
mol	molecular
$turb$	turbulent
I	first reaction
II	second reaction
III	third reaction
+	forward reaction
-	backward reaction

INTRODUCTION

CFD simulations of dispersed bubbly flow on the scale of technical equipment are feasible within the Eulerian two-fluid framework of interpenetrating continua. However, accurate numerical predictions rely on suitable closure models. To achieve predictive capability, all details of the closures have to be fixed in advance without reference to any measurement data for the problem under investigation.

Concerning the fluid dynamics of bubbly flows a baseline model has recently been proposed to this end and shown to work for a range of different applications in a unified manner. This provides a reliable background which is well suited to add more complex physics.

Concerning mass transfer in bubbly flows both with and without an accompanying chemical reaction only few studies have been performed to date. Hence, a generally accepted closure model for the mass transfer coefficient has not emerged yet. This is partly due to a lack of experimental data suitable for model validation. Such data should provide spatially resolved measurements of concentration together with the bubble size distribution and cover a certain range of parameters known to be relevant, i.e. bubble size and turbulent fluctuations.

The effect of a chemical reaction on the mass transfer is commonly described by an enhancement factor which depends on the type of the reaction. For a meaningful validation of closure models a reliable characterization of the reaction kinetics is required in this case as well.

In the present contribution we consider a recent experiment on the absorption of CO_2 in aqueous NaOH in a bubble column (Hlawitschka et al., 2017), which will be referred to as reactive case in the following. Fluid dynamical measurements have been conducted as well for CO_2 bubbles in water in the same column (Kovats et al., 2015, Rzehak et al., 2017), where effects of chemical reactions are vanishingly small, which is why this case will be referred to as non-reactive case. For both the non-reactive and the reactive case a comparison is made with Euler-Euler simulations using previously established closure models. Results for the non-reactive case have already been published (Rzehak et al., 2017) and a selection is shown for completeness here. Results for the reactive case are new.

DATA

An experiment for which both fluid dynamics and reactive mass transfer were investigated has been presented recently by (Kovats et al., 2015, Rzehak et al., 2017, Hlawitschka et al., 2017). The geometry considered (Fig.1) was that of a round bubble column with an inner diameter of 142 mm. Initially, the column was filled up to a height of 730 mm either with de-ionized water or with aqueous NaOH at a pH of 9.5. CO_2 gas was supplied through four needles arranged in a line, spaced by 22 mm, and extending by 13 mm into the column. The gas flow rate was set to 6.4 l/h and an average size of the generated bubbles of d_B = 2.72 mm resulted with a standard deviation of 0.33 mm. Even for the reactive case, this value did not vary appreciably throughout the column which means that the gas absorption rate is very low. The rise of the liquid surface due to the additional gas in the column was found negligible. The experiment was performed under ambient conditions.

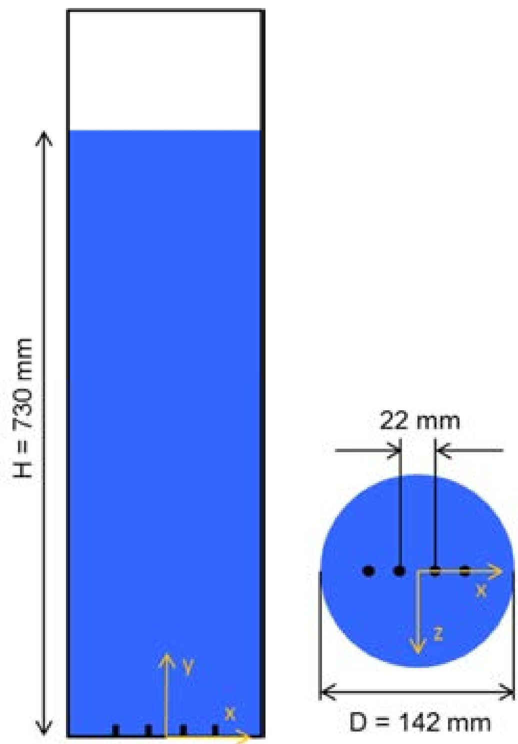

Figure 1: Schematic diagram of geometry.

Bubble location, velocity, and diameter were determined by shadowgraphy in a field of view extending up to a height of 300 mm with a depth of focus of ±20 mm about the *xy*-plane in which the needles are located. From the bubble location data gas fractions were obtained by counting the number of bubbles falling into each cell of a grid covering the measurement plane. For comparison with the Euler-Euler simulations it has to be kept in mind that these gas fractions pertain to a slab with the thickness of the depth of focus and a corresponding average has to be taken in the simulation results.

Liquid velocity and its fluctuations were measured by PIV in five separate fields of view covering the entire column height with some overlap. Two-dimensional fields are obtained again in the *xy*-plane and for the two velocity components *u* and *v* lying in this plane.

Information about the pH-value can be discerned from LIF measurements by a calibration of the detected fluorescence intensity. The *xy*-plane was resolved in four separate fields of view over the column height.

For further details on the measurements we refer to the original papers (Kovats et al., 2015, Rzehak et al., 2017, Hlawitschka et al., 2017).

MODELING

The entire model comprising multi-physics and chemistry is quite complex and space limitations preclude a full presentation. Detailed descriptions of modeling are available in previous works, i.e. Rzehak and Krepper (2013, 2015), Rzehak et al. (2014, 2015, 2017, 2017a), Rzehak and Kriebitzsch (2015), Ziegenhein et al. (2015, 2017), and Liao et al. (2016) for the fluid dynamics, Rzehak and Krepper (2016) for physical mass transfer and Krauß and Rzehak (2017, 2017a) for the chemical reactions and their effects on the mass transfer. In the following a brief summary is given, which emphasizes a few key issues concerning the reactive mass transfer.

The fluid dynamical part of the model comprises momentum exchange between the phases and liquid phase turbulence. The momentum exchange is governed by drag, (shear-) lift, wall (-lift), turbulent dispersion and virtual mass forces. The original works from which these correlations have been taken are summarized in Table 1. Turbulence is described by an SST-model common in single phase turbulence, which has been augmented by source terms describing the bubble-induced contribution (Rzehak and Krepper, 2013a).

For the mass transfer part, models are required for the mass transfer coefficient k_L and the turbulent diffusivity. Considering the resistance to mass transfer to be only on the liquid side, a correlation due to Brauer (1981) is applied, i.e.

$$k_L = \frac{D_{L,mol}^{CO_2}}{d_B}\left(2 + 0.015\ Re_B^{0.89} Sc_{L,mol}^{0.7}\right), \qquad (1)$$

with Reynolds and Schmidt numbers defined as $Re_B = |\mathbf{u}_L - \mathbf{u}_G| d_B \rho_L \mu_L^{-1}$ and $Sc_{L,mol} = \mu_L \left(\rho_L D_{L,mol}^{CO_2}\right)^{-1}$.

This correlation was derived based on an analysis of mass transfer measurements on single bubbles in the

Table 1: Summary of bubble force correlations.

force	reference
drag	Ishii and Zuber (1979)
shear lift	Tomiyama et al. (2002)
wall lift	Hosokawa et al. (2002)
turbulent dispersion	Burns et al. (2004)
virtual mass	constant coefficient $C^{VM} = 1/2$

wobbling regime which applies to gas bubbles of millimeter size in water.
The effective diffusivity in the liquid phase is the sum of a molecular contribution $D_{L,mol}^{CO_2}$ and a turbulent contribution $D_{L,turb}^{CO_2}$. The latter is calculated from the turbulent kinematic viscosity by means of a turbulent Schmidt number for which the simple but frequently used assumption is made to take it as unity, i.e.

$$Sc_{L,turb} = \frac{\mu_{L,turb}}{\rho_L D_{L,turb}^{CO_2}} = 1 \,. \tag{2}$$

The network of chemical reactions occurring during the absorption of CO_2 in aqueous NaOH is shown in Fig. 2. The relative importance of the two reaction pathways, hydroxylation (superscript I in Fig. 2) and hydration (superscript III in Fig. 2), depends on the pH-value. Hydroxylation dominates for pH > 10 and hydration dominates for pH < 8, while in between both reactions pathways are relevant (Kern, 1960). The need to include the hydration reaction to correctly capture the approach to the neutral point has been shown in Krauß and Rzehak (2017).
The effect of the chemical reactions on the mass transfer is modeled by an enhancement factor that depends on the type of reaction that occurs. Treating hydroxylation and hydration as independent parallel reactions (cf. van Swaaij and Versteeg, 1992) it can be seen that only the former is capable to cause a notable effect. Moreover, unless the temperature is increased or extra carbonate is added to the liquid, the equilibrium of reaction II lies far on the carbonate side so that the enhancement effect can be deduced from the effective overall reaction $CO_2 + 2\,OH^- \rightarrow CO_3^{\,2-} + H_2O$, which is an irreversible bimolecular reaction (Krauß and Rzehak, 2017). An expression for the enhancement factor for this case has been derived by DeCoursey (1974) based on the renewal model as

$$E = -\frac{Ha^2}{2(E_a - 1)} + \sqrt{\frac{Ha^4}{4(E_a - 1)^2} + E_a \frac{Ha^2}{(E_a - 1)} + 1} \,, \tag{3}$$

where the Hatta number is defined as

$$Ha = \frac{\sqrt{k_L^{I+} D_{L,mol}^{CO_2} C_L^{OH^-}}}{k_L} \tag{4}$$

and E_a gives the asymptotic limiting value for the enhancement factor of an instantaneous reaction.
Care has to be taken that a common approximation for the instantaneous enhancement factor E_a is not used outside its regime of validity which is restricted to large values. A fit formula that is applicable over a wide range of conditions has been proposed in Krauß and Rzehak (2017) and is used herein. With this fit formula, the enhancement factor converges to one for pH<11.5 which is why for the conditions of the present experiment no significant enhancement effect occurs.

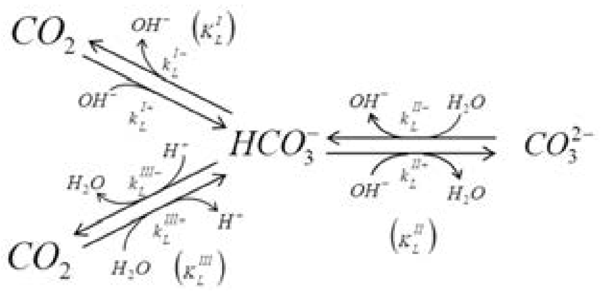

Figure 2: Reaction scheme of CO_2 in aqueous solution.

Correlations for reaction rates and physicochemical properties have been assembled in Rzehak and Krepper (2016) and Krauß and Rzehak (2017, 2017a).

SIMULATIONS

Simulations have been performed for both the non-reactive and the reactive cases using a custom version of ANSYS CFX 14.5. The simulations were run in transient (URANS) mode on the full 3D domain. For both cases the domain was discretized using a grid with 86720 cells, which was found sufficient by a previously performed mesh study (Rzehak et al., 2017a). For the non-reactive case the time-step was set to $1 \cdot 10^{-2}$ s, which guaranteed that the Courant-Friedrichs-Lewy number was always far below 1. For the reactive case smaller time-steps had to be used depending on the current pH-value, being lowered by hand from $5 \cdot 10^{-4}$ s to $1 \cdot 10^{-4}$ s as the simulation progressed. Time-averaged results have been averaged over a simulated physical time of 10 min discarding the initial transient until a statistically stationary state was attained. This time interval is sufficiently long that the resulting average does not change significantly anymore.
On the walls a no-slip condition holds for the continuous phase and a free-slip condition for the dispersed phase, assuming that direct contacts between the bubbles and the walls are negligible. To avoid the need to resolve the viscous sublayer, a single phase turbulent wall function assuming a smooth wall was used. For the mass fractions, the normal derivative vanishes on the walls as well as at the outlet at the top of the domain. In addition, a degassing condition was applied there, meaning an outlet condition for the dispersed phase and a free-slip and no-penetration condition for the continuous phase. The four needles were represented by point sources.
For the reactive case the continuous phase is considered as a mixture of sodium, hydroxide, bicarbonate and carbonate ions and carbon dioxide dissolved in water. While the initial concentrations of sodium and hydroxide ions were calculated with the initial pH-value of 9.5, all other concentrations were initially set to zero. The gas phase only consists of carbon dioxide. Bubble size distributions were narrow (Rzehak et al., 2017) and neither bubble coalescence and breakup nor shrinkage due to gas absorption was observed because the gas absorption rate was very small. Therefore a

monodisperse approximation with a constant bubble diameter of 2.72 mm was applied. Physicochemical properties were evaluated at atmospheric pressure and a temperature of 20°C.

RESULTS

Non-reactive case

For the non-reactive case, a statistically stationary state is attained after an initial transient when the gas flow is turned on. Thus, a time average of the experimental data is suitable for comparison with the Euler-Euler simulations. Since the simulations are run in URANS mode which allows to capture also time-dependent mean flows, such as e.g. bubble plume oscillations, a time average denoted as ⟨⟩ is also performed on the simulation results.

A comparison between measured and calculated gas fractions is shown in Fig. 3. As already noted, an additional spatial average corresponding to the depth of focus of the shadowgraphy system has been applied to the simulations. The agreement between experiment and simulation is quite good. Special emphasis should be placed on the four peaks of gas fraction which are of the same width and get lower but broader with increasing height. This proves the suitability of the non-drag force models summarized in Table 1. However, the total amount of gas is a bit too high in the simulation.

This is confirmed by the comparison of the simulated and experimentally determined gas velocities shown in Fig. 4. The simulated velocities are close to the experimental ones. Both the experiment and the simulation show slightly lower velocities at the lowest height of 50 mm than at the other two positions. For all three heights the velocity is almost constant over the central portion of the column and decreases near the walls, but overall the simulated values are slightly too low. The consequence of this difference is a higher mean residence time of the gas bubbles and thus a slightly higher gas fraction as demonstrated in Fig. 3.

A comparison for the axial component of the mean liquid velocity is shown in Fig. 5. Close to the inlet region four peaks of velocity are visible matching the four peaks of gas fraction in Fig. 3 which is because most momentum is exchanged in regions of high buoyancy and consequently high drag forces. The simulated velocity is somewhat lower than in the experiment which is in accordance with the slightly lower gas velocities of the simulation in Fig. 4. It may be noted that in the experiment the second needle from the right apparently produced a faster liquid stream than the others. Since no difference is seen for this needle in the gas fraction, the reason for this is unclear, but the effect may be taken as an estimate of the magnitude of factors which are hard to control in laboratory experiments and which will inevitably be present in technical applications. A slight reminiscence of the resulting peak in the liquid velocity persists up to the higher level of 600 mm. Nevertheless, in consideration of the asymmetry of the experimental velocity profile the agreement between the experiment and the simulation is quite good.

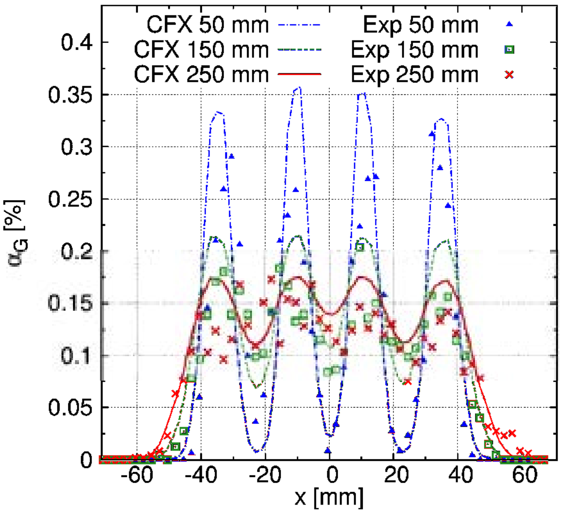

Figure 3: Comparison of gas fraction. Profiles at different heights as indicated in the legend.

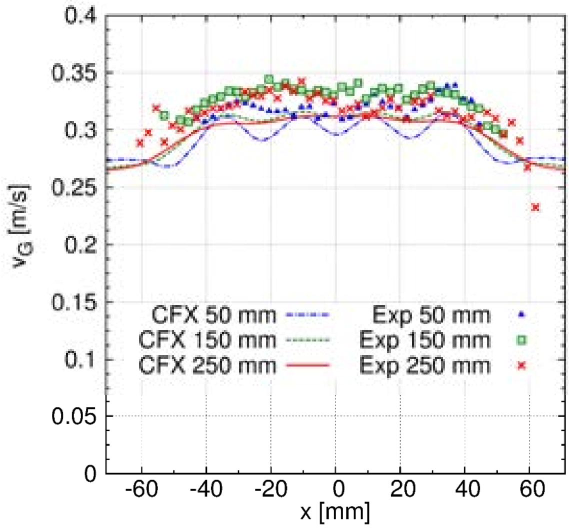

Figure 4: Comparison of gas velocity. Profiles at different heights as indicated in the legend.

Finally, the liquid velocity fluctuations are considered. For the simulations in URANS mode one has to take into account that there are two contributions to the covariance tensor of liquid velocity fluctuations $\mathbf{u}'_L\mathbf{u}'_L$: resolved and unresolved ones (Ziegenhein et al., 2015). The unresolved contribution is obtained from the averaged modeled turbulent kinetic energy k_L and is isotropic, while the resolved contribution is calculated from the time-dependent liquid velocity field and is anisotropic. The resulting expression is

$$\mathbf{u}'_L\mathbf{u}'_L = \left\langle \left(\mathbf{u}_L(t) - \mathbf{u}_L\right)\left(\mathbf{u}_L(t) - \mathbf{u}_L\right)\right\rangle + \frac{2}{3}\left\langle k_L(t)\right\rangle \mathbf{1} , \qquad (5)$$

where **1** denotes the identity tensor. Fig. 6 shows the square root of the liquid velocity fluctuations in the axial direction. For the simulations in addition to the total fluctuations, which are compared with the experimental data, the resolved and unresolved contributions are also given separately. Agreement

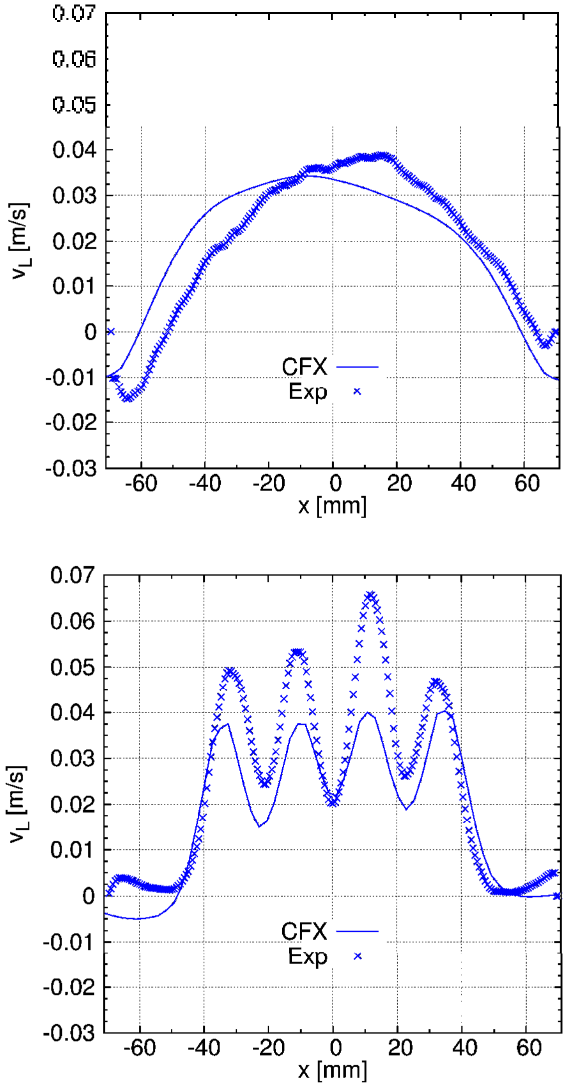

Figure 5: Comparison of axial liquid velocity. Profiles at different heights: bottom: H = 50 mm; top: H = 600 mm.

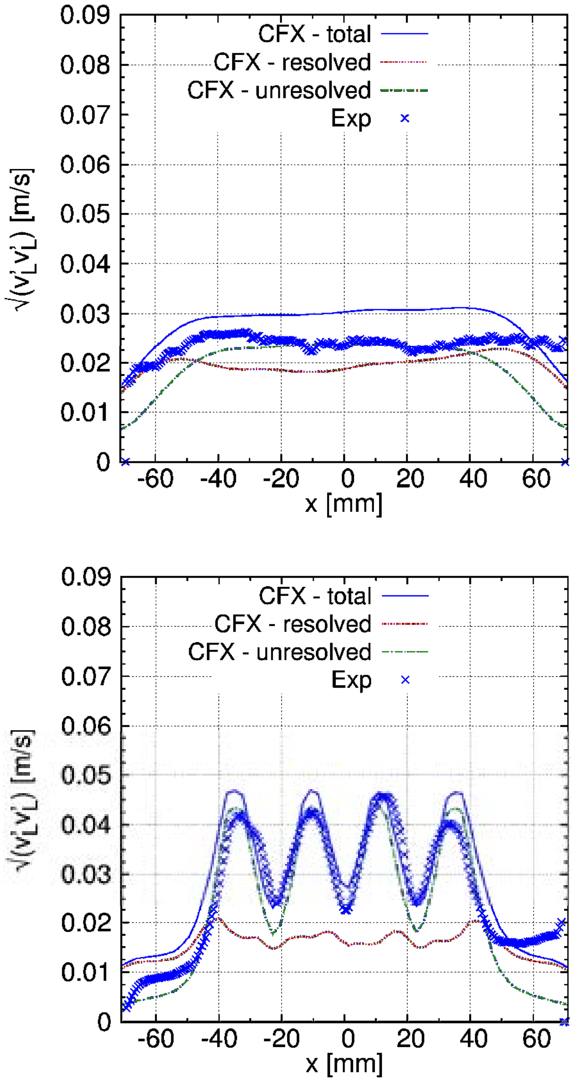

Figure 6: Comparison of axial liquid velocity fluctuations. Profiles at different heights: bottom: H = 50 mm; top: H = 600 mm.

between simulation and experiment is good for both levels. In addition, it is observed that near the inlet needles the unresolved contribution dominates over the resolved one, while at larger heights, both contributions are of similar magnitude. Once again, four peaks are observed near the inlet needles matching the peaks in gas volume fraction and liquid velocity. In those regions of high gas volume fractions and their consequently high drag forces high contributions of bubble-induced turbulence are obtained. Furthermore, high liquid velocity gradients exist, which lead to high shear-induced turbulence contributions. For the upper level, where gradients of gas fraction and liquid velocity are clearly reduced, both contributions to the unresolved turbulence are much smaller.

Reactive case

For the reactive case, the system behavior is time-dependent due to the accumulation of reaction products and dissolved carbon dioxide in the column. As an illustration of this time dependency 2D fields of the simulated pH-value are shown in Fig. 7 at different physical times. Near the inlet liquid is carried upwards by the rising bubbles. Due to the high pH-values in the lower part of the column the absorbed gas is transformed to carbonate ions by the hydroxylation reaction pathway. During the decrease in pH-value with increasing height the carbonate ions are converted to bicarbonate ions by the second backward reaction. Furthermore, the hydration of carbon dioxide starts, whereby the pH-value continues to decrease. At a height of ~250 mm accumulation of carbon dioxide by the liquid phase begins and the decrease in pH-value slows down. Near the outlet the slightly acidic liquid changes its direction of flow and moves downwards close to the column walls. This provides a continuous transport of fresh liquid downwards to the inlet needles until all of the liquid above ~250 mm has been converted to an acidic environment. Only then does the reaction spread out to the lower part of the column.

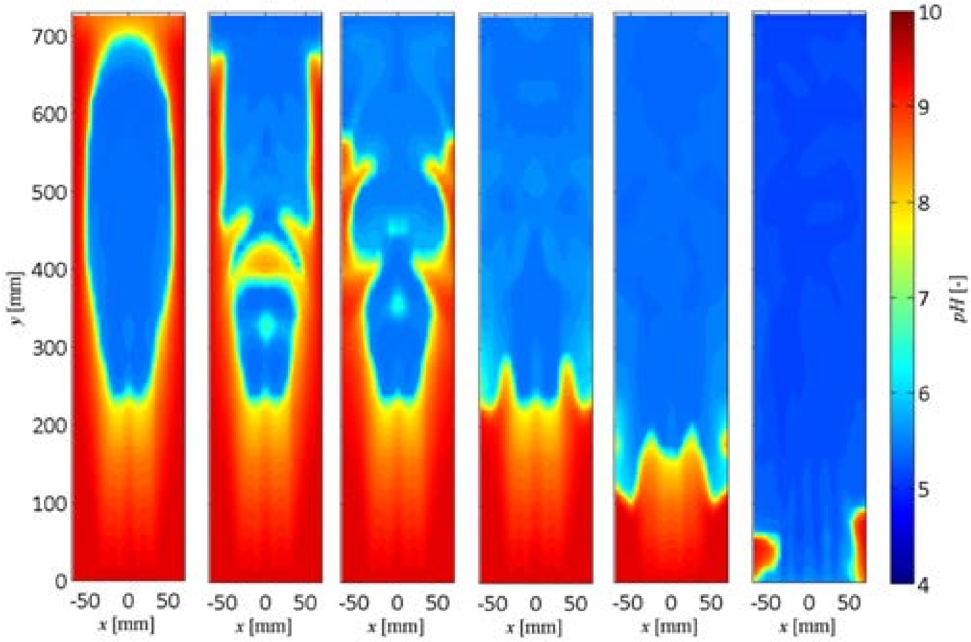

Figure 7: 2D fields of simulated pH-value. From left to right: simulation result after 11, 14, 18, 24, 34 and 60 s of gas supply.

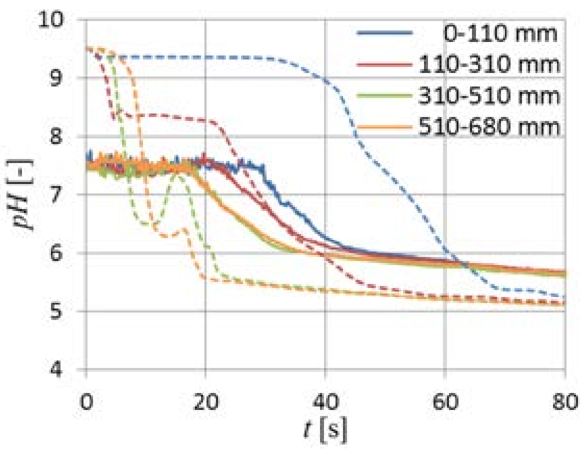

Figure 8: Comparison of the time-dependent pH-value, spatially averaged for the column height segments as indicated in the legend, between the simulation (dashed lines) and the experiment (solid lines). Note that the LIF method is limited to pH < ~7.6.

For a quantitative analysis, averages have been performed over the four column height segments corresponding to the separate fields of view in the experiment. The results are shown as the dashed lines in Fig. 8. It is seen that the drop in pH, which indicates the progress of the reactions, occurs first and almost simultaneously for the upper two segments from 310 mm to 680 mm. The segments from 110 mm to 310 mm and from 0 mm to 110 mm follow with a delay of ~20 s each.

Quantitatively big differences are seen between the simulation and the experimental results, which were processed analogously and are shown by the solid lines in Fig. 8. Note that only values of pH < ~7.6 are quantifiable by the LIF method applied here, because the fluorescence intensity is the same for all higher pH-values. The order in which the drop in pH occurs is the same in the experiment as in the simulation, but the starting times differ significantly. For the upper two sections it starts later in the experiment than in the simulations, for the second section from below at about the same time and in the lowest section it starts earlier in the experiment than in the simulation. In addition the pH curves level off at pH ≈ 6.0 in the experiment but only at pH ≈ 5.5 in the simulations which could be a result of differences in chemical equilibrium evoked by differing conditions, such as temperature or initial pH-value. In the experiment the four separate segments were investigated sequentially in separate runs which requires a multiple preparation of the initial solution. In fact, the initial pH-values were not exactly identical, but there were differences up to 0.3. Also the precise value of temperature was not recorded in the experiment. The small peaks in the simulated pH-values of the upper two sections at ~15 s are not observed in the experiment. They are caused by liquid of higher pH-values entering the measurement plane from other regions.

It must be noted that the deviations between the simulation and the experiment are substantially caused by experimental difficulties, in particular concerning the start-up process. The four needles do not start to supply gas simultaneously, but with considerable delays, which in addition are subject to large statistical variations. Therefore, the gas flow rate in the experiment does not change from zero to the nominal value instantaneously, but is ramped up over a time interval which is of the order of 7 to 20 s. In addition there are local variations of gas supply during this period which may have an impact on the bubble column hydrodynamics. Finally this ramp-up process is different for the different experimental runs from which the LIF data for the four segments were obtained. All of these effects could not be captured by the simulation where the gas supply starts instantaneously and for all needles simultaneously. To make a comparison, starting time for the experimental curves was chosen halfway in between the release of the first bubble by the first and the last needle.

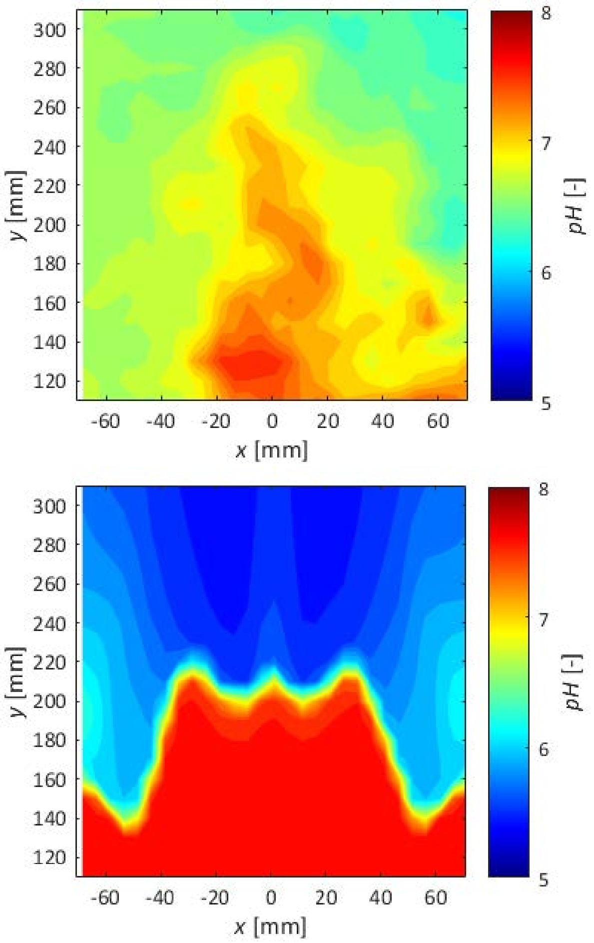

Figure 9: Comparison of 2D fields of the instantaneous pH-value between the simulation (bottom) and the experiment (top) at t = 30 s in the segment from 110 mm to 310 mm.

In Fig. 9, the instantaneous 2D fields of pH-value at t = 30 s of the experiment and the simulation are compared in the height segment from 110 mm to 310 mm. The highest pH-values of both fields are observed in the lower middle of the segment and decrease with increasing height. Slightly acidic liquid flows downwards next to the walls. The major difference between the simulation and the experiment is the significantly lower level of mixing in the simulation, which results in much stronger gradients of pH-value and therefore in substantial quantitative deviations.

In Fig. 10 the radially averaged pH-values at t = 30 s are plotted over the column height for both experiment and simulation. Note that the simulated pH-values have been limited to pH < ~7.6 in accordance with the sensitivity of the fluorescence to improve comparability. Both curves show a decrease in pH-value with increasing height which predominates at a height between 100 mm and 300 mm. However, according to the lower level of mixing in the simulation the decrease of the simulation is rather steep, whereas the decrease in the experiment is much more gradual. Moreover, the approximately constant pH-value for y > 300 mm is ~0.5 lower in the simulation than in the experiment. In addition to the aforementioned experimental difficulties this deviation could be again a result of differences in chemical equilibrium as already discussed above.

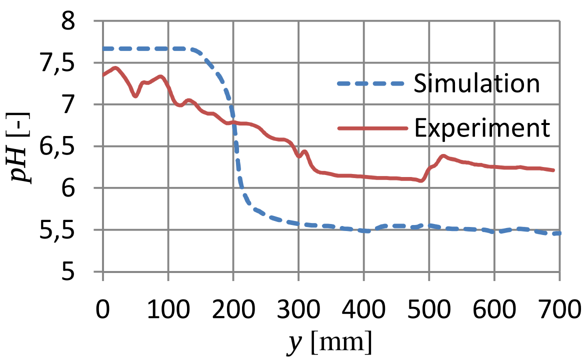

Figure 10: Comparison of radial averaged pH-value over height at t = 30 s.

In view of the good agreement of the time-averaged results for the non-reactive case, the shortcoming of the reactive modeling is thus likely to be produced by errors in the reproduction of the dynamical flow behavior and the resulting poor mixing of the liquid phase in the simulation. It is likely that the high level of mixing in the experiment is evoked by small scale turbulence which cannot be resolved by the URANS approach used here.

CONCLUSION

Simulations have been performed corresponding to a new experiment that comprises optical measurements of both fluid dynamics and reactive mass transfer. The Euler-Euler approach has been applied with closures that were previously established in independent investigations.

For the fluid dynamics, time-averaged results in the stationary state were investigated. Quite good agreement was found for the gas fraction, mean liquid velocity and turbulent fluctuations.

For the reactive mass transfer the ramp-up process of the chemisorption of carbon dioxide in sodium hydroxide solution was investigated. This ramp-up process provides stronger spatial differences in the concentration fields than the gas supply into a developed flow as studied in previous works, e.g. Darmana et al. (2007). Thus the configuration presently studied bears the possibility of a more conclusive model validation. While the potential of this approach can be confirmed from the qualitative similarities between simulation and experiment, the significant quantitative differences point to the need for its refinement.

In the course of the work it became apparent that the experiments were in some respects less well controlled than desirable for their use to validate CFD simulations. These issues are not completely obvious, hence the discussion may be useful to design future experiments with an increased reliability. In particular, for each experimental attempt crucial parameters like the initial pH-value and the ramp-up process of gas supply have to be identical for each repetition, especially when results from different runs are stitched together. Furthermore, the experimental error of the different measurement methods should be quantified in order to also access the quantitative model error.

Concerning the simulations, one may already draw the conclusion that the predicted mixing of chemical species is significantly too weak. This is most likely due to a lack of resolving smaller scale turbulent structures, which are expected to be mainly responsible for mixing. Improvement could be achieved by applying a large eddy simulation, which is more able to resolve these kinds of turbulent structures, but requires much higher computational effort than the URANS model used here. Using the identical model for the setup of Darmana et al. (2007), a rectangular bubble column with higher superficial gas velocities, such severe problems were not observed. Presumably this is because the flow structures responsible for mixing in that case were fairly big and reasonably resolved by the URANS method, although some relatively minor deviations remained (Krauß and Rzehak, 2017a).

ACKNOWLEDGEMENT

This work has been carried out in the frame of a research project (GZ: RZ 11/1-1) within the DFG Priority Programme 1740: "Reactive Bubbly Flows" funded by the DFG.

REFERENCES

BRAUER, H., (1981), "Particle/fluid transport processes", *Prog. Chem. Eng.,* **19**, 81–111.

BURNS, A.D., FRANK, T., HAMILL, I. and SHI, J.-M., (2004), "The Favre averaged drag model for turbulence dispersion in Eulerian multi-phase flows", *5th Int. Conf. on Multiphase Flow* (ICMF2004), Yokohama, Japan.

DARMANA, D., HENKET, R., DEEN, N. and KUIPERS, J., (2007), "Detailed modelling of hydrodynamics, mass transfer and chemical reactions in a bubble column using a discrete bubble model: Chemisorption of CO2 into NaOH solution, numerical and experimental study", *Chem. Eng. Sci.,* **62**, 2556–2575.

DeCOURSEY, W. J., (1974), "Absorption With Chemical Reaction: Development Of A New Relation For The Danckwerts Model", *Chem. Eng. Sci.*, **29**, 1867–1872.

HLAWITSCHKA, M., KOVÁTS, P., ZÄHRINGER, K. and BART, H.-J., (2017), "Simulation and experimental validation of reactive bubble column reactors", *Chem. Eng. Sci.*, in press.

HOSOKAWA, S., TOMIYAMA, A., MISAKI, S. and HAMADA, T., (2002), "Lateral Migration of Single Bubbles Due to the Presence of Wall", *ASME Joint U.S.-European Fluids Engineering Division Conference* (FEDSM 2002), Montreal, Canada.

ISHII, M. and ZUBER, N., (1979), "Drag coefficient and relative velocity in bubbly, droplet or particulate flows", *AIChE J.,* **25**, 843–855.

KERN, D. M., (1960), "The hydration of carbon dioxide", *J. Chem. Educ.,* **37**, 14–23.

KOVÁTS, P., THÉVENIN, D. and ZÄHRINGER, K., (2015), "Fluid-dynamical Characterization of a Bubble Column for Investigation of Mass-transfer", *Conference on Modelling Fluid Flow* (CMFF'15), Budapest, Hungary.

KRAUSS, M. and RZEHAK, R., (2017), "Reactive absorption of CO2 in NaOH: Detailed study of enhancement factor models", *Chem. Eng. Sci.*, **166**, 193–209.

KRAUSS, M. and RZEHAK, R., (2017a), "Reactive absorption of CO2 in NaOH: An Euler-Euler simulation study", *Chem. Eng. Tech.*, submitted.

LIAO, J., ZIEGENHEIN, T. and RZEHAK, R., (2016), „Bubbly flow in an airlift column: a CFD study", *J. Chem. Tech. Biotech.,* **91**, 2904–2915.

RZEHAK, R. and KREPPER, E., (2013), "Closure Models for turbulent bubbly flows: A CFD study", *Nucl. Eng. Des.,* **265**, 701–711.

RZEHAK, R. and KREPPER, E., (2013a), "CFD modeling of bubble-induced turbulence", *Int. J. Multiphase Flow,* **55**, 138–155.

RZEHAK, R., KREPPER, E., ZIEGENHEIN, T. and LUCAS, D., (2014), „A baseline model for monodisperse bubbly flows", *10th International Conference on CFD in Oil & Gas, Metallurgical and Process Industries* (CFD2014), Trondheim, Norway.

RZEHAK, R. and KREPPER, E., (2015), "Bubbly flows with fixed polydispersity: validation of a baseline closure model", *Nucl. Eng. Des.,* **287**, 108–118.

RZEHAK, R. and KRIEBITZSCH, S., (2015), „Multiphase CFD-simulation of bubbly pipe flow: A code comparison", *Int. J. Multiphase Flow,* **68**, 135–152.

RZEHAK, R., KREPPER, E., LIAO, Y., ZIEGENHEIN, T., KRIEBITZSCH, S. and LUCAS, D., (2015), Baseline model for the simulation of bubbly flows", *Chem. Eng. Tech.,* **38**, 1972–1978.

RZEHAK, R., (2016), "Modeling of mass-transfer in bubbly flows encompassing different mechanisms", *Chem. Eng. Sci.*, **151**, 139–143.

RZEHAK, R. and KREPPER, E., (2016), "Euler-Euler simulation of mass-transfer in bubbly flows", *Chem. Eng. Sci.*, **155**, 459–468.

RZEHAK, R., ZIEGENHEIN, T., KRIEBITZSCH, S., KREPPER, E. and LUCAS, D., (2017), "Unified modeling of bubbly flows in pipes, bubble columns, and airlift columns", *Chem. Eng. Sci.*, **157**, 147–158.

RZEHAK, R., KRAUSS, M., KOVÁTS, P. and ZÄHRINGER, K., (2017a), "Fluid dynamics in a bubble column: New experiments and simulations", *Int. J. Multiphase Flow*, **89**, 299–312.

TOMIYAMA, A., TAMAI, H., ZUN, I. and HOSOKAWA, S., (2002), "Transverse migration of single bubbles in simple shear flows", *Chem. Eng. Sci.,* **57**, 1849–1858.

ZIEGENHEIN, T., RZEHAK, R. and LUCAS, D., (2015), "Transient simulation for large scale flow in bubble columns", *Chem. Eng. Sci.,***122**, 1–13.

ZIEGENHEIN, T., RZEHAK, R., MA, T. and LUCAS, D., (2017), "Towards a unified approach for modeling uniform and non-uniform bubbly flows", *Can. J. Chem. Eng.,* **95**, 170–179.